MOX-Report No. 82/2020

A seamless, extended DG approach for hyperbolic-parabolic problems on unbounded domains

Vismara, F; Benacchio, T.; Bonaventura, L.

MOX, Dipartimento di Matematica
Politecnico di Milano, Via Bonardi 9 - 20133 Milano (Italy)

mox-dmat@polimi.it http://mox.polimi.it

A seamless, extended DG approach for hyperbolic-parabolic problems on unbounded domains

Federico Vismara*, Tommaso Benacchio, Luca Bonaventura

December 10, 2020

MOX – Modelling and Scientific Computing,
Dipartimento di Matematica, Politecnico di Milano
Via Bonardi 9, 20133 Milano, Italy
f.vismara@tue.nl, tommaso.benacchio@polimi.it,
luca.bonaventura@polimi.it

Keywords: Laguerre functions; hyperbolic equations; parabolic equations; discontinuous Galerkin methods; open boundary conditions.

AMS Subject Classification: 65M60, 65M70, 65Z99, 76M10, 76M22.

*Present address: CASA, Technische Universiteit Eindhoven, The Netherlands

Abstract

We propose and analyze a seamless extended Discontinuous Galerkin (DG) discretization of hyperbolic-parabolic equations on semi-infinite domains. The semi-infinite half line is split into a finite subdomain where the model uses a standard polynomial basis, and a semi-unbounded subdomain where scaled Laguerre functions are employed as basis and test functions. Numerical fluxes enable the coupling at the interface between the two subdomains in the same way as standard single domain DG interelement fluxes. A novel linear analysis on the extended DG model yields stability constraints on the finite subdomain grid size that get tighter for increasing values of the Péclet number. Errors due to the use of different sets of basis functions on different portions of the domain are negligible, as highlighted in numerical experiments with the linear advection-diffusion and viscous Burgers' equations. With an added damping term on the semi-infinite subdomain, the extended framework is able to efficiently simulate absorbing boundary conditions without additional conditions at the interface. A few modes in the semi-infinite subdomain are found to suffice to deal with outgoing single wave and wave train signals, thus providing an appealing model for fluid flow simulations in unbounded regions.

1 Introduction

The correct modelling of evolution problems over arbitrarily large regions has a wide range of applications in computational physics and poses several still unsolved challenges. An especially relevant application area is atmospheric modelling, where the region of interest to forecasts - typically, the troposphere and lower stratosphere - should not feature spurious reflections of upwardly propagating waves generated by the computational model lid, see, e.g., [9,17,18]. At the same time, as computational resources enable raising the lid, an accurate description of upper atmosphere phenomena is of paramount practical interest and the goal of fully integrated space weather models is increasingly being discussed, see, e.g., [1, 16].

Approximations over arbitrarily large regions usually rely on the creation of an artificial boundary separating the region of interest from an external region. Analytical approaches, e.g., [11, 12, 15], attempt to impose conditions at the artificial boundary in order to let outgoing perturbations propagate without spurious reflections. However, these conditions can be difficult to determine and computationally expensive, and may require *ad hoc* information on the outgoing signal.

An alternative approach is provided by numerical techniques based on absorbing (or sponge) layers. These are buffer regions placed next to the artificial boundary where perturbations leaving the computational domain are damped to a prescribed external solution by an artificial dissipation term. The choice of the parameters to be employed in these regions, however, is non-trivial and the corresponding buffers may be quite large and entail substantial computational costs. A complete review of the proposed approaches for open boundary conditions is beyond the scope of this paper. Comprehensive reviews can be found, for example, in [2, 5, 6, 8, 13, 19].

In [6, 7], a numerical approach to open boundary conditions was proposed, based on the use of scaled Laguerre functions [21–23, 25, 27] for spectral approximations on the semi-infinite line, coupled to finite volume or finite element discretizations on a finite domain. Different approaches were used on either side of the artificial boundary, and only the hyperbolic case was considered. In addition, the stability analysis in [7] only concerned the discretization on the semi-infinite subdomain.

This paper expands and completes the previously proposed approach by presenting two major improvements. First, the method is extended to hyperbolic-parabolic conservation laws, thus showing that all relevant terms of standard computational fluid dynamics

models are amenable to a discretization based on scaled Laguerre functions. Second, the hyperbolic-parabolic model equations are discretized in a completely seamless way, using a discontinuous Galerkin (DG) finite element formulation that relies on scaled Laguerre functions as both basis and test functions on the semi-infinite portion, along with Gauss-Laguerre-Radau quadrature rules for numerical integration.

The resulting extended DG approach and its numerical stability on the entire half line are analyzed in the case of a linear advection-diffusion equation, by considering several options for the polynomial basis and quadrature rules. Scaled Laguerre functions and Gauss-Laguerre-Radau quadrature formulae prove to be the most stable in all hydrodynamic regimes.

Numerical validations of the proposed method are carried out for the linear advection-diffusion and the viscous Burgers' equation. First, a relatively large number of basis functions are in the semi-infinite portion of the domain, in order to evaluate the errors introduced by considering different bases on either side of the finite/semi-infinite interface. By taking as reference a standard single-domain DG discretization, spurious reflections are found to be of negligible entity. A reaction damping term is then introduced in the semi-infinite layer, in order to simulate the propagation of an isolated Gaussian initial datum and boundary generated wave train from the finite subdomain into the semi-infinite subdomain, where they are erased using a decreasing number of Laguerre basis functions. Few basis functions suffice to absorb outgoing signals with minimal reflections and low computational cost, thereby providing an efficient implementation of an absorbing layer.

The outline of the paper is as follows. Section 2 contains the model equation and outlines the numerical discretization. Stability properties of the proposed method are analyzed in detail in Section 3, and Section 4 contains the results of the numerical experiments. The final Section 5 draws conclusions, discussing possible extensions and future work. The Appendix A summarizes the analysis of different possible discretizations on the semi-infinite domain, based on either scaled Laguerre functions or polynomials or on different choices for the numerical quadrature rules. As already shown in [7], some of these alternatives are shown to be more problematic in the advection-dominated case.

2 The extended DG discretization approach

We consider as a model problem the one-dimensional nonlinear hyperbolic-parabolic conservation law for the unknown c

$$\frac{\partial c}{\partial t} + \frac{\partial f(c)}{\partial z} = \frac{\partial}{\partial z}\left(\mu(z,t)\frac{\partial c}{\partial z}\right) + s(c,z,t) \tag{1}$$

for $z \in [0,+\infty)$ and $t \in [0,T]$. We assume that the diffusion coefficient μ is a smooth function of its variables and that there are two positive constants μ_0 and μ_1 such that

$$0 < \mu_0 \leq \mu(z,t) \leq \mu_1 \qquad \forall z \in [0,+\infty), \quad \forall t > 0. \tag{2}$$

For simplicity, we only consider here Dirichlet boundary conditions

$$c(0,t) = g_0(t) \qquad \lim_{z\to+\infty} c(z,t) = 0. \tag{3}$$

We refer to [24] for a comprehensive analysis of other boundary conditions in the linear advection-diffusion case.

Next, drawing on the approach of [6, 7] we split the domain as $\mathbb{R}^+ = [0,L] \cup [L,+\infty)$ and introduce an extended DG finite element discretization on $\mathbb{R}^+$ using a standard polynomial basis on $[0,L]$ and the scaled Laguerre functions as both basis and test functions on $[L,+\infty)$. More specifically, on the $[0,L]$ interval a mesh of N non-overlapping elements K_m of size $\Delta z_m \leq h$ is considered, such that $[0,L] = \bigcup_{m=1}^{N} K_m$. The center of the generic element K_m is denoted by z_m, while $z_{m\pm1/2}$ denote its boundary points. The affine local maps $z = Z_m(\xi) = \xi\Delta z_m/2 + z_m$ map the master element $\hat{K} = [-1,1]$ onto each K_m. For each non-negative integer p, we then denote by $\mathbb{P}_p$ the set of all polynomials of degree less or equal to p on $\hat{K}$. We also define $\mathbb{P}_p(K_m) = \left\{w : w = v \circ Z_m^{-1}, \quad v \in \mathbb{P}_p\right\}$. For each polynomial degree p, the discontinuous finite element spaces are defined as:

$$V_h^p = \left\{v \in L^2([0,L]) : v|_{K_m} \in \mathbb{P}_p(K_m) \quad m = 1,\ldots,N\right\}. \tag{4}$$

The bases of $\mathbb{P}_p(K_m)$ are obtained from Legendre polynomials as follows. First, for $\xi \in \hat{K}$, Legendre polynomials are defined by the recurrence relation:

$$L_{k+1} = \frac{2k+1}{k+1}\xi L_k(\xi) - \frac{k}{k+1}L_{k-1}(\xi), \qquad k = 1,2,\ldots \tag{5}$$

$$L_0(\xi) = 1, \quad L_1(\xi) = \xi. \tag{6}$$

Legendre polynomials form an orthogonal basis for polynomials on $\hat{K}$ since

$$\int_{-1}^{1} L_k(\xi)L_l(\xi)d\xi = \frac{2}{2k+1}\delta_{kl}. \tag{7}$$

For each element K_m, $m = 1, \ldots, N$ we then denote by $\phi_j^m(z), j = 0, \ldots, p$ the basis and test functions given by

$$\phi_l^m(z) = \sqrt{2l+1}L_l\Big(2\frac{z - z_m}{\Delta z_m}\Big). \tag{8}$$

Notice that the normalization is chosen so that

$$\int_{z_{m-\frac{1}{2}}}^{z_{m+\frac{1}{2}}} \phi_k^m(z)\phi_l^m(z)\, dz = \Delta z_m \delta_{kl}. \tag{9}$$

Therefore, the solution of (1) will be represented on each subinterval K_m as

$$c(z,t) \approx \sum_{j=0}^{p} c_m^{(j)}(t)\phi_j^m(z), \qquad z \in K_m \tag{10}$$

and standard Gauss-Legendre formulae will be used to discretize the resulting integrals. For the semi-infinite interval $K_\infty = [L, +\infty)$, we consider the scaled Laguerre functions as modal basis. The possible alternatives are discussed and analyzed in [7] for the purely hyperbolic case and in Appendix A of this paper for the hyperbolic-parabolic case. More specifically, defining scaled Laguerre polynomials on $[0, +\infty)$ by

$$(k+1)\mathscr{L}_{k+1}^{\beta}(x) = (2k+1-\beta x)\mathscr{L}_k^{\beta}(x) - k\mathscr{L}_{k-1}^{\beta}(x), \tag{11}$$

$$\mathscr{L}_0^{\beta}(x) = 1,\ \mathscr{L}_1^{\beta}(x) = 1 - \beta x, \tag{12}$$

scaled Laguerre functions are defined by

$$\hat{\mathscr{L}}_k^{\beta}(x) = e^{-\beta x/2}\mathscr{L}_k^{\beta}(x). \tag{13}$$

for the scaling factor $\beta > 0$, and are a complete orthogonal system in $L^2(\mathbb{R}^+)$, such that

$$\int_0^{+\infty} \hat{\mathscr{L}}_k^{\beta}(x)\hat{\mathscr{L}}_l^{\beta}(x)dx = \frac{1}{\beta}\delta_{kl}. \tag{14}$$

We then define

$$\phi_j^{\infty}(z) = \hat{\mathscr{L}}_j^{\beta}(z - L), \quad j = 0, \ldots, q \tag{15}$$

for which the analog of (9) holds

$$\int_L^{+\infty} \phi_k^{\infty}(z)\phi_l^{\infty}(z)\, dz = \frac{1}{\beta}\delta_{kl}. \tag{16}$$

and we assume that

$$c(z,t) \approx \sum_{j=0}^{q} c_{\infty}^{(j)}(t)\phi_j^{\infty}(z) \qquad z \in K_{\infty}. \tag{17}$$

For the resulting integrals, Gauss-Laguerre-Radau quadrature will be employed, see [6] for the definition. Approximation (17) amounts to say that the restriction of the numerical approximation of c to K_{∞} will be sought in the linear space V_{∞}^{q} spanned by the functions defined in (15).

Therefore, the global finite element space employed in the proposed extended DG discretization can be identified with $V_h^{p,q} = V_h^p \oplus V_{\infty}^q$. For $v \in V_h^{p,q}$ we can then introduce the jump and average operators as (see, e.g., [4])

$$[\![v(z)]\!] = v(z^-) - v(z^+), \qquad \{v(z)\} = \frac{1}{2}(v(z^-) + v(z^+)) \tag{18}$$

and we remark that for $u, v \in V_h^{p,q}$ one has

$$[\![uv]\!] = \{u\}\,[\![v]\!] + \{v\}\,[\![u]\!]. \tag{19}$$

The extended DG discretization then involves integration of equation (1) against a test function $v \in V_h^{p,q}$, integrating by parts and imposing for $m = 1, \ldots, N$ the appropriate continuity constraints at the interelement boundaries. Setting

$$N_{\infty} = \{1, 2, \ldots, N, \infty\}, \tag{20}$$

denoting by $\sigma > 0$ the stabilization parameter for the DG approximation of the parabolic terms, and redefining the jump and average operators at $z = 0$ so as to account for the boundary conditions, we

obtain the following weak extended DG formulation of the problem:

$$\begin{aligned}\sum_{m\in N_\infty}\int_{K_m}\frac{\partial c}{\partial t}v dz = &-\sum_{m=1}^{N}\hat{f}_{m+1/2}\left[\!\left[v\left(z_{m+1/2}\right)\right]\!\right]\\ &+\sum_{m\in N_\infty}\int_{K_m}f(c)v'dz-\sum_{m\in N_\infty}\int_{K_m}\mu\frac{\partial c}{\partial z}v'dz\\ &+\sum_{m=0}^{N}\left\{\mu\left(z_{m+1/2}\right)\frac{\partial c}{\partial z}\left(z_{m+1/2}\right)\right\}\left[\!\left[v\left(z_{m+1/2}\right)\right]\!\right]\\ &+\sum_{m=0}^{N}\left\{\mu\left(\left(z_{m+1/2}\right)v'\left(z_{m+1/2}\right)\right\}\left[\!\left[c\left(z_{m+1/2}\right)\right]\!\right]\right.\\ &-\sum_{m=0}^{N}\frac{\sigma}{\Delta z_m}\left[\!\left[c\left(z_{m+1/2}\right)\right]\!\right]\left[\!\left[v\left(z_{m+1/2}\right)\right]\!\right]\\ &+\sum_{m\in N_\infty}\int_{K_m}svdz\\ &+\mu(0,t)v'(0)g_0(t)+f(g_0(t))v(0).\end{aligned}\tag{21}$$

At $z=L$, the limit from the left of the approximate solution is computed as $\sum_{j=0}^{p}c_N^{(j)}(t)\phi_j^N(L)$, while the limit from the right is computed as $\sum_{j=0}^{q}c_\infty^{(j)}(t)$, according to the approximations (10), (17), respectively. Among the many possible formulations for the parabolic terms, for definiteness we choose that corresponding to the Symmetric Interior Penalty Galerkin method (SIPG), see, e.g., [3, 26] and the review in [20]. Furthermore, the Rusanov numerical flux is employed for the hyperbolic terms, so that

$$\begin{aligned}\hat{f}_{m+1/2}=&\frac{1}{2}\left[f\left(c^+_{h,m+1/2}\right)+f\left(c^-_{h,m+1/2}\right)\right]\\ &-\frac{\Lambda_{m+1/2}}{2}\left(c^+_{h,m+1/2}-c^-_{h,m+1/2}\right),\end{aligned}\tag{22}$$

where the time dependency is omitted for simplicity,

$$\Lambda_{m+1/2}=\max\left(\left|\frac{df}{dc}\left(c^+_{h,m+1/2}\right)\right|,\left|\frac{df}{dc}\left(c^-_{h,m+1/2}\right)\right|\right),\tag{23}$$

and $c^+_{h,m+1/2}=c_h\left(z^+_{m+1/2}\right)$, $c^-_{h,m+1/2}=c_h\left(z^-_{m+1/2}\right)$.
We can now define the bilinear form

$$a: V_h^{p,q}\times V_h^{p,q}\times[0,+\infty)\to\mathbb{R}\ \text{ as}\tag{24}$$

$$
\begin{aligned}
a(w,v,t) = & \sum_{m\in N_\infty} \int_{K_m} \mu \frac{\partial w}{\partial z} v' dz \\
& - \sum_{m=0}^{N} \left\{ \mu\left(z_{m+1/2},t\right) \frac{\partial w}{\partial z}\left(z_{m+1/2}\right) \right\} \left[\!\left[v\left(z_{m+1/2}\right) \right]\!\right] \\
& - \sum_{m=0}^{N} \left\{ \mu\left(z_{m+1/2},t\right) v'\left(z_{m+1/2}\right) \right\} \left[\!\left[w\left(z_{m+1/2}\right) \right]\!\right] \\
& + \sum_{m=0}^{N} \frac{\sigma}{\Delta z_m} \left[\!\left[w\left(z_{m+1/2}\right) \right]\!\right] \left[\!\left[v\left(z_{m+1/2}\right) \right]\!\right],
\end{aligned}
\tag{25}
$$

and the nonlinear function $b : V_h^{p,q} \times V_h^{p,q} \to \mathbb{R}$ as

$$
\begin{aligned}
b(w,v) = & \sum_{m=1}^{N} f\left(w\left(z_{m+1/2}\right)\right) \left[\!\left[v\left(z_{m+1/2}\right) \right]\!\right] \\
& - \sum_{m\in N_\infty} \int_{K_m} f(w) v' dz - \sum_{m\in N_\infty} \int_{K_m} s(w) v dz.
\end{aligned}
\tag{26}
$$

We also introduce $g : V_h^{p,q} \times V_h^{p,q} \to \mathbb{R}$, $h : V_h^{p,q} \times V_h^{p,q} \to \mathbb{R}$ as

$$
g(w,v,t) = -\mu(L,t) v'(L) w(L) + \frac{\sigma}{\Delta z_N} v(L) w(L) \tag{27}
$$

$$
h(w,v) = -f(w(L)) v(L) \tag{28}
$$

and the linear operator $L : V_h^{p,q} \times [0,+\infty) \to \mathbb{R}$

$$
L(v,t) = \mu(0,t) v'(0) g_0(t) + \frac{\sigma}{\Delta z_1} v(0) g_0(t) + f(g_0(t)) v(0), \tag{29}
$$

which is related to the Dirichlet condition at the left endpoint $z = 0$. The extended DG weak formulation can then be written more compactly as follows:

For all $t > 0$, find $c_h(t) \in V_h^{p,q}$ such that, $\forall v \in V_h^{p,q}$,

$$
\begin{aligned}
\int_0^{+\infty} \frac{\partial c_h}{\partial t} v dz = & - a(c_h, v, t) - b(c_h, v) \\
& + L(v,t) + g(c_h, v, t) + h(c_h, v).
\end{aligned}
\tag{30}
$$

Approximating c_h using (10) and (17), and taking $v = \phi_j^m$ and $v = \phi_k^\infty$, one obtains a set of equations for the discrete degrees of freedom $c_m^{(j)}$ $j = 0, \ldots, p, m = 1, \ldots, N$ $c_\infty^{(k)}$ $k = 0, \ldots, q$. Collecting these in two time-dependent vectors $\mathbf{c}_{Dg} \in \mathbb{R}^{N(p+1)}$ and $\mathbf{c}_{Lg} \in \mathbb{R}^{q+1}$,

one obtains the systems

$$\begin{aligned}\frac{d\mathbf{c}_{Dg}}{dt} &= \mathbf{A}_{Dg}\mathbf{c}_{Dg} + \mathbf{A}_{Dg,Lg}\mathbf{c}_{Lg} \\ &\quad + \mathbf{b}_{Dg}(\mathbf{c}_{Dg}) + \mathbf{h}_{Dg}(\mathbf{c}_{Dg}, \mathbf{c}_{Lg}) + \mathbf{g}_0(t)\end{aligned} \tag{31}$$

$$\begin{aligned}\frac{d\mathbf{c}_{Lg}}{dt} &= \mathbf{A}_{Lg}\mathbf{c}_{Lg} + \mathbf{A}_{Lg,Dg}\mathbf{c}_{Dg} \\ &\quad + \mathbf{b}_{Lg}(\mathbf{c}_{Lg}) + \mathbf{h}_{Lg}(\mathbf{c}_{Dg}, \mathbf{c}_{Lg}).\end{aligned} \tag{32}$$

The time-dependent matrices $\mathbf{A}_{Dg}$ and $\mathbf{A}_{Lg}$ result from the discretization of the diffusion operator in the interior of the $[0, L]$ and $[L, +\infty)$ subdomains, respectively. The coupling matrices $\mathbf{A}_{Dg,Lg}$ and $\mathbf{A}_{Lg,Dg}$ result from the discretization of the diffusion operator involving discrete degrees of freedom of both subdomains. The nonlinear functions $\mathbf{b}_{Dg}$ and $\mathbf{b}_{Lg}$ result from the discretization of the hyperbolic part and source terms in the interior of the $[0, L]$ and $[L, +\infty)$ subdomains, respectively. The term $\mathbf{g}_0(t)$ is associated with boundary conditions at $z = 0$, while the coupling nonlinear functions $\mathbf{h}_{Dg}(\mathbf{c}_{Dg}, \mathbf{c}_{Lg})$ and $\mathbf{h}_{Lg}(\mathbf{c}_{Dg}, \mathbf{c}_{Lg})$ result from the discretization of the hyperbolic part involving discrete degrees of freedom of both subdomains.
Next, we define the global unknown vector as

$$\mathbf{c}(t) = (\mathbf{c}_{Dg}(t), \mathbf{c}_{Lg}(t))^T \in \mathbb{R}^{N(p+1)+q+1}, \tag{33}$$

and the global vectors

$$\mathbf{b}(\mathbf{c}(t)) = (\mathbf{b}_{Dg}(\mathbf{c}_{Dg}(t)), \mathbf{b}_{Lg}(\mathbf{c}_{Lg}(t)))^T \in \mathbb{R}^{N(p+1)+q+1} \tag{34}$$

$$\mathbf{h}(\mathbf{c}) = (\mathbf{h}_{Dg}(\mathbf{c}_{Dg}, \mathbf{c}_{Lg}), \mathbf{h}_{Lg}(\mathbf{c}_{Dg}, \mathbf{c}_{Lg}))^T \in \mathbb{R}^{N(p+1)+q+1} \tag{35}$$

$$\mathbf{g}(t) = (\mathbf{g}_{Dg}(t), 0, \ldots, 0)^T \in \mathbb{R}^{N(p+1)+q+1}. \tag{36}$$

Defining the global extended DG matrix

$$\mathbf{A}(t) = \begin{pmatrix} \mathbf{A}_{Dg}(t) & \mathbf{A}_{Dg,Lg}(t) \\ \mathbf{A}_{Lg,Dg}(t) & \mathbf{A}_{Lg}(t) \end{pmatrix} \in \mathbb{R}^{(N(p+1)+q+1)\times(N(p+1)+q+1)}, \tag{37}$$

the extended DG semi-discrete formulation reads

$$\frac{d\mathbf{c}(t)}{dt} = \mathbf{A}(t)\mathbf{c}(t) + \mathbf{b}(\mathbf{c}(t)) + \mathbf{h}(\mathbf{c}(t)) + \mathbf{g}(t). \tag{38}$$

The matrix $\mathbf{A}$ is the discretization of the diffusion term, the vector $\mathbf{b}$ is the discretization of the non-linear advective part and the optional source-reaction term, the vector $\mathbf{h}$ contains the flux exchange at the interface $z = L$ by means of the application of the Rusanov

flux to the flux function f, and the vector $\mathbf{g}$ encodes the Dirichlet condition at the left endpoint $c(0) = a(t)$. We remark that, because of the vectors $\mathbf{b}$ and $\mathbf{h}$, problem (38) is non-linear. However, if the functions f and s in (1) are linear, then $\mathbf{b}(\mathbf{c}(t))$ and $\mathbf{h}(\mathbf{c}(t))$ can be written as the product between a matrix and the unknown vector $\mathbf{c}(t)$. In this case, (38) is a linear system of equations.
The semi-discrete extended DG formulation (38) can then be discretized in time by any standard method for the numerical solution of ODE systems. In this paper, we use the Crank-Nicolson method for the linear test problems considered in Section 4. For the non-linear problems, a second order implicit-explicit (IMEX) method is used, that is described, e.g., in [10, 14]. The terms associated with the diffusion process are treated implicitly, as they can entail otherwise rather restrictive stability constraint on the time step size, while the terms associated with the hyperbolic conservation law are treated explicitly.

3 Stability analysis

In order to study the numerical stability of the global semi-discrete extended DG formulation (38), we consider the special case of the linear, constant coefficient, advection-diffusion equation:

$$\frac{\partial c}{\partial t} + u\frac{\partial c}{\partial z} = \mu\frac{\partial^2 c}{\partial z^2} + s(c, z, t) \tag{39}$$

i.e. equation (1) with $f(c) = uc$, $\mu(z, t) \equiv \mu$, $\mu, u \in \mathbb{R}^+$, and in the homogeneous case the source term $s \equiv 0$.

We study the spectrum of the extended DG matrix $\mathbf{A}$ (37) for the discretization (38) of (39) as a function of the Péclet number $Pe = u\mathcal{L}/\mu$, where $\mathcal{L}$ is a reference length scale. More specifically, we fix $\mathcal{L} = 1$, $\beta = 1$ for the scaling Laguerre parameter, $\mu = 1$, $u = Pe\mu$. We consider a uniform mesh on the finite subdomain and empirically study under which conditions on the element size Δz the discretization is stable, in the sense that $\max(\Re[\lambda(\mathbf{A})]) \leq 0$. This study is carried out for a range of values of the maximum DG polynomial degree p, number of Laguerre basis functions q, and the values $\sigma = 20$ and $\sigma = 200$ of the penalization parameter.

Results of the analysis are reported in Table 1. It can be observed that larger values of σ allow for larger sub-intervals without losing stability. In addition, critical values of the spacing Δz are found to be independent of the number q of basis functions in the semi-infinite subdomain at fixed polynomial degree p in the finite subdomain. If the Péclet number is small enough – approximately less than 100 –

the spectrum of $\mathbf{A}$ has negative real part regardless of the spacing Δz, and a few sub-intervals in the finite subdomain $[0, L]$ are enough to make the scheme stable. By contrast, large values of Pe require a fine grid in $[0, L]$ to prevent spurious growth caused by eigenvalues with positive real part. As a consequence, sufficiently large values of N will be considered in the following numerical validations.

Table 1: Critical values Δz_{cr} of the finite subdomain grid spacing Δz for the stability of $\mathbf{A}$ in the extended DG scheme, $\mu = 1$, $u = Pe\mu$, $\sigma = 200$ (left), $\sigma = 20$ (right).

q	p	Pe		
		100	500	1000
180	3	1/2	1/4	1/9
	2	1/2	1/8	1/20
	1	1/2	1/9	1/20
90	3	1/2	1/5	1/13
	2	1/2	1/9	1/21
	1	1/2	1/10	1/21
50	3	1/2	1/6	1/10
	2	1/2	1/10	1/22
	1	1/2	1/10	1/21
20	3	1/2	1/5	1/8
	2	1/2	1/10	1/22
	1	1/2	1/10	1/21

q	p	Pe		
		100	500	1000
180	3	1/6	1/21	1/40
	2	1/7	1/35	1/73
	1	1/6	1/30	1/61
90	3	1/5	1/20	1/34
	2	1/7	1/37	1/75
	1	1/5	1/30	1/61
50	3	1/4	1/18	1/30
	2	1/7	1/37	1/75
	1	1/5	1/30	1/61
20	3	1/5	1/15	1/27
	2	1/8	1/38	1/76
	1	1/7	1/30	1/61

4 Numerical experiments

We present here the results of several numerical tests with the extended DG approach described in the previous sections.

First, a number of validation tests are carried out, considering both linear and non-linear model problems. The tests assess the accuracy of the extended DG scheme by comparing it with a stand-alone, single-domain reference DG discretization on a wider domain. Errors are computed using a relatively large number of modes in the semi-infinite subdomain of the extended DG scheme, and the wider domain for the stand-alone reference run also covers part of the semi-infinite subdomain.

Next, we add a damping reaction term in the semi-infinite subdomain to simulate an absorbing layer. We show that the extended

DG scheme efficiently damps signals leaving the finite subdomain with negligible reflections into the finite region.

The experiments consider the linear advection-diffusion equation with constant coefficients (39), both in the non-homogeneous case ($s \neq 0$) and the homogeneous case ($s = 0$), and the nonlinear, homogeneous viscous Burgers' equation with constant viscosity, i.e., equation (1) with $f(c) = c^2/2$, $\mu(z,t) \equiv \mu \in \mathbb{R}^+$, and $s = 0$.

Errors are computed on the finite region $[0, L]$ using a suitable Gaussian quadrature rule on the sub-intervals K_m, whose width is $\Delta z = L/N$ for all $m = 1, \ldots, M$. In particular, we introduce the discrete norms

$$\|c_h\|_{L^2} = \sqrt{\sum_{m=1}^{N} \frac{\Delta z}{2} \sum_{k=1}^{ng} \left[c_h \left(\frac{\Delta z}{2} x_k + z_m \right) \right]^2 w_k} \tag{40}$$

$$\|c_h\|_{L^1} = \sum_{m=1}^{N} \frac{\Delta z}{2} \sum_{k=1}^{ng} \left| c_h \left(\frac{\Delta z}{2} x_k + z_m \right) \right| w_k \tag{41}$$

$$\|c_h\|_{L^\infty} = \max_{m=1,\ldots,N} \max_{k=1,\ldots,ng} \left| c_h \left(\frac{\Delta z}{2} x_k + z_m \right) \right|, \tag{42}$$

where $\{x_k\}_{k=1}^{ng}$ and $\{w_k\}_{k=1}^{ng}$ are the Gaussian nodes and weights on the reference interval $[-1, 1]$, with ng the number of quadrature points. Absolute errors with respect to a reference solution are defined as

$$\mathcal{E}_{L^r} = \|c_h - c_{ref}\|_{L^r}, \quad r \in 1, 2, \infty \tag{43}$$

where c_h and c_{ref} are the numerical and the reference solution, respectively; the latter may be either the exact solution or a single-domain DG discretization. In some tests we will be also interested in relative errors with respect to the reference solution c_{ref} defined as

$$\mathcal{E}^{rel}_{L^r} = \frac{\|c_h - c_{ref}\|_{L^r}}{\|c_{ref}\|_{L^r}}, \quad r \in 1, 2, \infty. \tag{44}$$

4.1 Validation of the extended DG scheme coupling strategy

We start by testing the proposed method for the linear advection-diffusion equation with constant coefficients (39). We first consider the non-homogeneous case by setting $s \neq 0$, assuming an exact solution $c(z,t) = ze^{-z}\sin^2(z-t)$, and computing the right-hand side analytically. We run the scheme for a variable number of modes q in the semi-infinite subdomain, also setting $N = 100$, $L = 2\,\mathrm{m}$, $p = 2$,

$\mu = 1\,\mathrm{m}^2/\mathrm{s}$, $u = 2Pe\mu$, and a final time $T = 10\,\mathrm{s}$ with $n = 200$ time steps. In order to minimize errors at the interface, the value of β is chosen in such a way that the distance between the first and the second node in the semi-infinite subdomain matches the grid spacing Δz in the finite subdomain. Relative errors L^1, L^2 and L^∞ errors at time T with respect to the exact solution due to the use of different sets of basis functions in the finite and semi-infinite subdomains are below $5 * 10^{-6}$ using at least 20 modes, below $3 * 10^{-3}$ using 10 modes, and a few percent using 5 modes, thus displaying spectral convergence in space (Table 2).

Table 2: Relative L^1, L^2 and L^∞ errors as functions of the number of modes q of the extended DG scheme with respect to the exact solution, linear non-homogeneous advection-diffusion equation. $\Delta t = 0.005\,\mathrm{s}$, $\Delta z = 0.02\,\mathrm{m}$, $C = 0.25$.

q	β	$\mathcal{E}_2^{\mathrm{rel}}$	$\mathcal{E}_1^{\mathrm{rel}}$	$\mathcal{E}_\infty^{\mathrm{rel}}$
5	30	5.40E-02	5.43E-02	7.93E-02
10	16	2.39E-03	2.46E-03	3.23E-03
20	8	3.30E-06	4.14E-06	2.86E-06
40	4	3.28E-06	4.12E-06	2.85E-06
80	2	3.28E-06	4.12E-06	2.85E-06

In a second test, we examine the accuracy of the extended DG scheme as a function of the Péclet number, Pe. We choose $N = 100$, $\beta = 1$, $q = 180$ that match the grid spacing across the interface between the two subdomains and maximize accuracy in the semi-infinite subdomain. Relative errors with respect to the exact solution are below $4 * 10^{-4}$ both in the advection-dominated and in the diffusion-dominated regimes (Table 3). The accuracy appears to decrease slightly for large values of Pe. We assume this to be related to the stability issues of the modal Laguerre discretization with Neumann boundary conditions discussed in the Appendix A.
Next, we validate the extended DG approach in the homogeneous case. We consider a Gaussian initial datum:

$$c_0(z) = \exp\left[-\left(\frac{z - z_c}{\sigma_c}\right)^2\right]. \tag{45}$$

The interface is located at $L = 10\,\mathrm{m}$ and the initial hump is placed inside the bounded interval $[0, L]$ by choosing $z_c = 8\,\mathrm{m}$. The velocity is $u = 1\,\mathrm{m/s}$ and the final time is $T = 4\,\mathrm{s}$, so that the peak of the Gaussian crosses the interface, and the other parameters are $\Delta t = 0.02\,\mathrm{s}$, $q = 40$ modes in the semi-infinite region, $N = 500$ subintervals for the DG scheme, so that $\Delta z = 0.02\,\mathrm{m}$. As the model

Table 3: Relative L^1, L^2 and L^∞ errors as functions of Pe of the extended DG scheme with respect to the exact solution, linear non-homogeneous advection-diffusion equation. $\Delta z = 0.01\,\mathrm{m}$, $q = 180$, $\Delta t = 0.05\,\mathrm{s}$.

Pe	$\mathcal{E}_2^{\mathrm{rel}}$	$\mathcal{E}_1^{\mathrm{rel}}$	$\mathcal{E}_\infty^{\mathrm{rel}}$
0.001	2.65E-04	3.16E-04	2.23E-04
10	4.69E-05	4.63E-05	5.15E-05
100	4.13E-06	4.54E-06	4.94E-06
500	8.28E-06	1.01E-05	9.20E-06
1000	3.81E-05	4.50E-05	3.83E-05

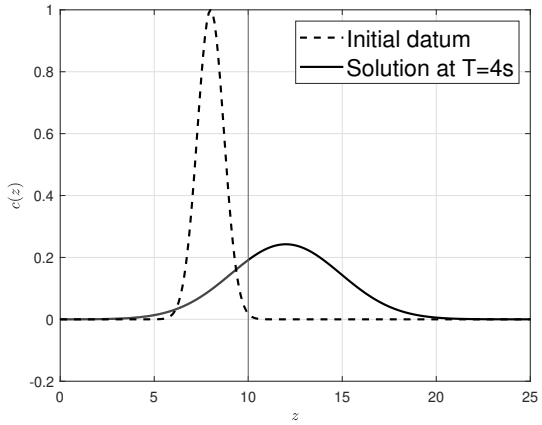

Figure 1: Numerical solution of the linear homogeneous advection-diffusion equation. Dashed line: initial datum. Solid line: numerical solution with the extended DG scheme at $T = 4\,\mathrm{s}$. $z_c = 8\,\mathrm{m}$, $\sigma_c = 1\,\mathrm{m}$, $q = 40$, $\beta = 4$, $\Delta z = 0.02\,\mathrm{m}$, $\Delta t = 0.02\,\mathrm{s}$, $\mu = 1\,\mathrm{m}^2/\mathrm{s}$, $u = 1\,\mathrm{m}/\mathrm{s}$.

evolves, the initial hump expands and its amplitude decreases because of diffusion (Figure 1). Relative errors in the finite subdomain $[0, 10\,\mathrm{m}]$ are computed for the extended DG scheme with respect to a single-domain DG solution run on $[0, 50\,\mathrm{m}]$. For $q = 10$ modes in the semi-infinite subdomain, relative errors are below a few percent, while for $q = 40$ they lower to around 10^{-10} (Table 4).

In a final validation test, we consider the case of the viscous Burgers' equation. The initial datum is the Gaussian profile $c_0(z) = \exp\left(-(z-3)^2\right)$, with the interface placed at $z = 3\,\mathrm{m}$. As time t evolves, the profile moves rightwards increasing its steepness – using the viscosity value $\mu = 0.05\,\mathrm{m}^2/\mathrm{s}$ no oscillations are observed until the final time $T = 1\,\mathrm{s}$. The extended DG scheme compares well with a reference solution computed by a single-domain DG discretization

Table 4: Relative L^1, L^2 and L^∞ errors in $[0, 10\,\mathrm{m}]$ of the extended DG discretization with respect to a single-domain DG discretization, linear homogeneous advection-diffusion equation. $z_c = 8\,\mathrm{m}$, $\Delta z = 0.02\,\mathrm{m}$, $\Delta t = 0.02\,\mathrm{s}$, $C = 1$.

q	β	σ_c	$\mathcal{E}_2^{\mathrm{rel}}$	$\mathcal{E}_1^{\mathrm{rel}}$	$\mathcal{E}_\infty^{\mathrm{rel}}$
10	16	1	1.90E-02	1.11E-02	3.79E-02
		2	1.97E-02	1.13E-02	4.10E-02
		0.5	1.87E-02	1.11E-02	3.70E-02
40	4	1	4.63E-09	2.31E-09	5.76E-08
		2	3.70E-09	2.83E-09	5.63E-09
		0.5	2.47E-09	1.94E-09	2.88E-09

on $[0, 10\,\mathrm{m}]$ (Figure 2).

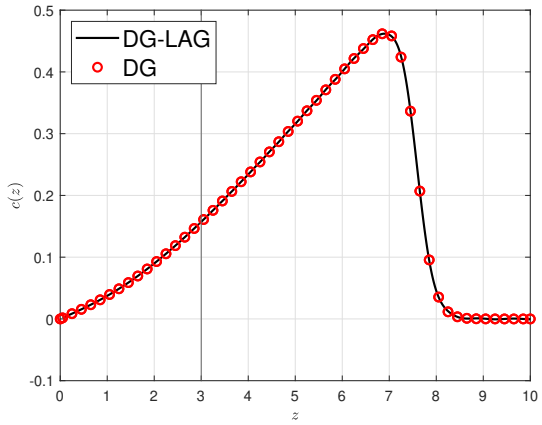

Figure 2: Numerical solution at $T = 1\,\mathrm{s}$ of the viscous Burgers' equation with Gaussian initial datum $q_0(z) = \exp\left(-(z-3)^2\right)$, $N = 30$, $q = 60$, $\Delta t = 10^{-6}\,\mathrm{s}$. Black line: extended DG scheme. Red circles: Single-domain DG discretization.

SSince the closed form of the solution is not available, we compute the errors with respect to a stand-alone DG discretization on a larger domain with the same spacing Δz. The finite/semi-infinite interface in the extended DG scheme is placed at $L = 3\,\mathrm{m}$ and the model is run until $T = 10\,\mathrm{s}$, with $\Delta t = 10^{-2}\,\mathrm{s}$. The cases of $N = 15$ and $N = 30$ subintervals in the finite subdomain are considered, varying the number of modes in the semi-infinite subdomain, and, accordingly, the scaling parameter β so that the distance between the first two nodes matches the grid spacing in $[0, L]$. The stand-alone single-domain DG reference solution for error computation is

obtained on the interval $[0, 10\text{m}]$. A small number of Laguerre modes are found to suffice to keep the coupling errors in the bounded subdomain $[0, L]$ below a few percent (Table 5).

Table 5: Relative L^1, L^2 and L^∞ errors in $[0, 3\,\text{m}]$ of the extended DG discretization with respect to a single-domain DG discretization, viscous Burgers' equation. $T = 10\,\text{s}$, $\Delta t = 10^{-2}\,\text{s}$, $N = 15$.

N	q	β	$\mathcal{E}_2^{\text{rel}}$	$\mathcal{E}_1^{\text{rel}}$	$\mathcal{E}_\infty^{\text{rel}}$
15	10	1.6	1.98E-02	7.80E-03	4.07E-02
	20	0.85	2.51E-02	1.04E-02	5.03E-02
	40	0.45	2.65E-02	1.17E-02	5.17E-02
	80	0.23	2.62E-02	1.18E-02	5.07E-02
30	10	3.6	6.81E-04	4.60E-04	9.18E-04
	30	1.2	5.62E-04	3.82E-04	7.59E-04
	60	0.6	6.36E-04	4.31E-04	7.96E-04
	100	0.36	6.76E-04	4.61E-04	8.77E-05

4.2 Efficiency of the extended DG scheme in absorbing layer tests

The second set of tests assesses the performance of the extended DG scheme in the absorption of perturbations leaving the finite subdomain when an artificial damping term $-\gamma c$, with $\gamma \geq 0$, is added to the model equations' right-hand side on the the semi-infinite subdomain $[L, +\infty)$. As in [6, 7] we choose a sigmoid of the form

$$\gamma(z) = \frac{\Delta\gamma}{1 + \exp\left(\dfrac{\alpha L_0 - z + L}{\sigma_D}\right)}, \tag{46}$$

where $\Delta\gamma$ is the sigmoid amplitude, $\alpha \in [0, 1]$ the position of the sigmoid inside the absorbing layer, L_0 the spatial extension of the semi-infinite region, i.e. the distance between the first and the last Gauss-Laguerre-Radau nodes, and σ_D the sigmoid steepness. As in [6, 7] we set $\alpha = 0.3\ m^{-1}$ and $\sigma_D = L_0/18$.

In a first experiment, we consider the linear advection-diffusion equation (39) and analyze the damping of a Gaussian profile defined by (45) and initially placed inside the finite region $[0, L]$. To this end, we place the interface at $L = 1000\,\text{m}$, set the initial data parameters $z_c = 750\,\text{m}$, $\sigma_c = 50\,\text{m}$, and $\mu = 1\,\text{m}^2/\text{s}$ and $u = 1\,\text{m/s}$. The crest moves across the finite region, crosses the interface and is damped in the semi-infinite region. Spurious reflections into the finite region,

measured as absolute errors of the computed solution in the finite region taking the absence of perturbation as reference, are below 10^{-3} for a range of values for the semi-infinite Laguerre modes q, finite subdomain subintervals N, and number of time steps n – and below 10^{-5} for the smallest $q = 5$ (Table 6).

Table 6: Absolute L^2, L^1 and L^∞ residual errors in the finite region for the damping of a Gaussian perturbation with the extended DG scheme, linear advection-diffusion equation. $C = 0.33$, $p = 2$, $T = 500\,\mathrm{s}$.

q	N	n	β	$\mathcal{E}_2$	$\mathcal{E}_1$	$\mathcal{E}_\infty$
40	400	600	1/28	9.51E-05	1.34E-04	1.03E-04
30			1/21	5.98E-06	1.18E-05	6.73E-06
20			2/29	2.58E-05	4.25E-05	2.70E-05
10			2/15	1.85E-06	6.84E-06	1.28E-06
5			1/4	1.52E-06	6.19E-06	8.15E-07
30	300	450	1/28	3.55E-04	4.99E-04	3.53E-04
20			1/19	2.59E-04	3.63E-04	2.59E-04
10			1/10	5.00E-06	1.18E-05	4.59E-06
5			11/60	1.67E-06	6.57E-06	1.03E-06
20	250	375	1/23	2.59E-04	3.63E-04	2.59E-04
10			1/12	5.00E-06	1.18E-05	4.59E-06
5			1/6	1.67E-06	6.57E-06	1.03E-06
10	200	300	1/15	4.56E-05	6.83E-05	3.84E-05
5			1/7	1.95E-06	7.48E-06	1.31E-06

Next, we consider a wave train case, obtained by imposing a Dirichlet boundary condition $c(0,t) = A\sin(2\pi k/Tt)$ at the left endpoint $z = 0$. The initial condition is $c_0 = 0$. The wave train is generated at $z = 0$, crosses the finite region $[0, L]$ and is damped by the absorbing layer, where we set $\Delta\gamma = 2A$. Numerical parameters are set as $L = 500\,\mathrm{m}$, $\mu = 1\,\mathrm{m}^2/\mathrm{s}$, $u = 1\,\mathrm{m/s}$, $T = 5000\,\mathrm{s}$, and $n = 16000$ time steps. On a range of choices for the wave number, amplitude, and Laguerre modes q, the extended DG scheme absorbs outgoing perturbations with relative errors computed in $[0, L]$ of less than 10^{-4} for $q = 15$, and at most $1.3 * 10^{-3}$ for $q = 5$, with respect to a reference single-domain DG solution on $[0, 2L]$ (Figure 3, Tables 7 and 8). Results are comparable with those obtained in [7] for the inviscid shallow water system with a different coupling approach. The efficiency of the tool is competitive – for $q = 5$, less than a hundredth for $N = 600$, and less than five thousandths for $N = 1200$, of the computational cost is due to the absorbing layer.

Finally, we consider the Burgers' equation. We place the interface at $L = 30\,\mathrm{m}$, and center an initial Gaussian profile inside

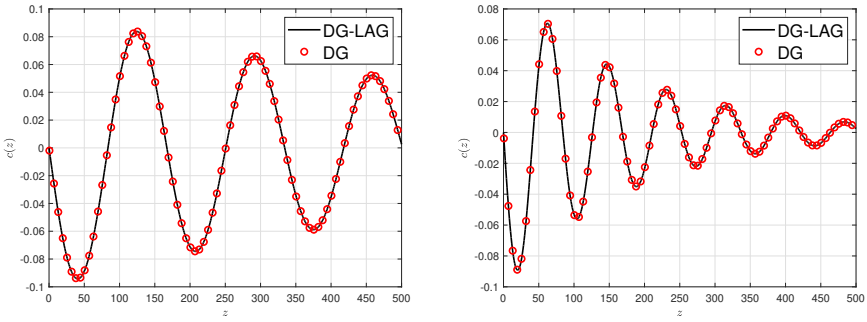

Figure 3: Damping of a wave train with wavenumber $k = 30$ (left), $k = 60$ (right), linear advection-diffusion equation. Solid line: extended DG scheme. Red circles: single-domain DG scheme. $A = 0.1\,\mathrm{m}$, $q = 30$, $N = 600$, $\beta = 0.143$, $T = 5000\,\mathrm{s}$, $n = 16000$.

Table 7: Damping of a wave train, linear advection-diffusion equation. Relative L^2, L^1 and L^∞ errors in $[0, L]$ of the extended DG solution with respect to a single-domain DG solution, $q = 15$ modes in the semi-infinite subdomain. $L = 500\,\mathrm{m}$, $p = 1$, $\mu = 1\,\mathrm{m}^2/\mathrm{s}$, $u = 1\,\mathrm{m/s}$, $T = 5000\,\mathrm{s}$, $n = 16000$.

A	k	N	β	$\mathcal{E}_2^{\mathrm{rel}}$	$\mathcal{E}_1^{\mathrm{rel}}$	$\mathcal{E}_\infty^{\mathrm{rel}}$
0.025	30	600	0.286	1.67E-06	2.25E-05	1.30E-07
	60	1200	0.571	1.10E-07	1.18E-08	1.31E-06
0.05	30	600	0.286	2.25E-06	1.78E-07	2.98E-05
	60	1200	0.571	2.55E-07	2.11E-08	3.23E-06
0.1	30	600	0.286	2.15E-06	1.85E-07	2.62E-05
	60	1200	0.571	4.74E-07	3.92E-08	5.99E-06

Table 8: Damping of a wave train, linear advection-diffusion equation. Relative L^2, L^1 and L^∞ errors in $[0, L]$ of the extended DG solution with respect to a single-domain DG solution, $q = 5$ modes in the semi-infinite subdomain. $L = 500\,\mathrm{m}$, $p = 1$, $\mu = 1\,\mathrm{m}^2/\mathrm{s}$, $u = 1\,\mathrm{m/s}$, $T = 5000\,\mathrm{s}$, $n = 16000$.

A	k	N	β	$\mathcal{E}_2^{\mathrm{rel}}$	$\mathcal{E}_1^{\mathrm{rel}}$	$\mathcal{E}_\infty^{\mathrm{rel}}$
0.025	30	600	0.74	9.23E-05	6.74E-06	1.30E-03
	60	1200	1.48	7.57E-06	7.57E-07	5.74E-05
0.05	30	600	0.74	4.23E-05	3.11E-06	5.91E-04
	60	1200	1.48	1.01E-05	1.03E-06	7.73E-05
0.01	30	600	0.74	3.15E-05	2.35E-06	4.41E-04
	60	1200	1.48	1.36E-05	1.44E-06	9.93E-05

the bounded region ($z_c = 25\,\mathrm{m}$, $\sigma_c = 1\,\mathrm{m}$). We run the extended DG scheme until $T = 3600\,\mathrm{s}$, when most of the initial perturbation has left the bounded region. Residual errors in the finite region $[0, L]$ with the extended DG scheme with respect to a single-domain DG solution on $[0, 10L/3]$ are below one percent for as few as $q = 5$ modes in the semi-infinite subdomain (Table 9). Qualitatively equivalent results are obtained when placing the initial data at the interface, $z_c = 30\,\mathrm{m}$ (not shown).

Table 9: Damping of a Gaussian profile initially centred at $z_c = 25\,\mathrm{m}$, viscous Burgers' equation. Relative L^2, L^1 and L^∞ errors in $[0, L]$ of the extended DG scheme compared with a single-domain DG solution. $T = 3600\,\mathrm{s}$, $\Delta t = 0.1\,\mathrm{s}$, $\Delta\gamma = 2$, $\sigma_c = 1\,\mathrm{m}$.

q	β	$\mathcal{E}_2^{rel}$	$\mathcal{E}_1^{rel}$	$\mathcal{E}_\infty^{rel}$
60	0.06	2.25E-03	1.15E-02	5.54E-04
40	0.09	2.24E-03	1.14E-02	5.50E-04
20	0.175	2.17E-03	1.10E-02	5.34E-04
10	0.34	1.96E-03	9.95E-03	4.83E-04
5	0.68	1.54E-03	7.76E-03	3.84E-04

5 Conclusions and perspectives

This paper proposed an extended DG approach for the numerical simulation of nonlinear hyperbolic-parabolic problems on unbounded domains. Built on earlier developments of coupled DG-Laguerre discretizations for purely hyperbolic systems, the scheme models a finite portion of the semi-infinite half-line using standard Legendre basis functions and the adjacent unbounded portion using scaled Laguerre basis functions.

Compared to a standard DG discretization, the extended DG scheme only differs for the presence of two off-diagonal terms in the system matrix, representing the numerical fluxes at the finite/semi-infinite interface. The new framework improves on previous endeavours that used bespoke coupling strategies, and provides a completely seamless coupling approach.

A linear analysis of the extended DG scheme in terms of the Péclet number identified stability thresholds on the grid spacing in the finite subdomain. The constraints become more stringent for increasingly advection-dominated flows and smaller values of the penalization parameter of the DG discretization in the finite subdomain. The analysis and numerical experiments used scaled

Laguerre basis functions, Gauss-Laguerre-Radau quadrature in the unbounded subdomain, and Dirichlet boundary conditions. Results covering other possible options are reported in [24] and are summarized in the Appendix, corroborating the findings for the standalone Laguerre scheme in a purely hyperbolic framework [7]. To the best of the authors' knowledge, a stability analysis on numerical schemes using different sets of basis functions as the one presented in this work is not currently available in the literature.

The correctness of the extended DG scheme, particularly regarding the finite/semi-infinite interface fluxes, was validated in a series of numerical experiments with the linear homogeneous and non-homogeneous advection-diffusion equation and the nonlinear viscous Burgers' equation. By comparison with a standard single domain implementation, spurious signals due to the presence of different basis functions are of negligible entity on a range of spatial resolutions, thereby complementing and strengthening results obtained with hyperbolic systems in [6, 7].

In tests where the semi-infinite subdomain featured a reactive damping term, the extended DG scheme displayed compelling performance in efficiently absorbing outgoing waves in linear and non-linear models. A very small number of Laguerre modes, both in absolute terms and as a proportion of the total computational load, was sufficient to damp single Gaussian signals and wave trains without spurious phenomena spoiling the simulation in the finite subdomain. Relative errors with respect to a single-domain DG scheme are small enough to make the extended DG scheme an interesting technique for the discretization of fluid dynamics problems on unbounded domains.

The results achieved in this work offer a number of perspectives for future investigation. First, a similar extended DG approach can be developed coupling a strong form, nodal DG discretization on the finite domain to the strong form, nodal approach with scaled Laguerre functions for the semi-infinite domain, a choice that displayed stability advantages in the large Péclet number case. The scheme can then be implemented in multiple dimensions, using tensor product-based discretization approaches on semi-infinite strips or circular domains, where the problem is discretized using the extended DG scheme in the vertical or radial direction and a discontinuous Galerkin approach in the horizontal or azimuthal direction. Such a model may find applications, for example, in the modelling of the solar corona. The extension to systems of parabolic equations or to non-linear diffusion may be considered, such as are found in turbulence modelling. From a more theoretical perspective, the pos-

sibility to prove inf-sup conditions for the extended DG approach could also be investigated.

Acknowledgements

This work summarizes and extends results obtained by the first author (F.V.) in his Master's Thesis in Mathematical Engineering [24], discussed at Politecnico di Milano in 2020 and prepared under the supervision of the other two authors. T.B. and L.B. have been supported by the ESCAPE-2 project of the Horizon 2020 research and innovation programme (grant agreement No 800897).

A Alternative discretizations on the semi-infinite subdomain

We summarize here the results presented in [24] on the analysis of various Laguerre-based discretizations of the advection-diffusion equation with constant coefficients on $\mathbb{R}^+ = [0, +\infty)$. For the purpose of deriving some discretizations, it can be helpful to reformulate equation (39), which we report here for convenience,

$$\frac{\partial c}{\partial t} + u\frac{\partial c}{\partial z} = \mu\frac{\partial^2 c}{\partial z^2} \tag{47}$$

as a system of first order equations

$$\begin{aligned} &\frac{\partial c}{\partial t} - \mu\frac{\partial v}{\partial z} + uv = 0 \\ &\frac{\partial c}{\partial z} - v = 0. \end{aligned} \tag{48}$$

We assume that solutions vanish at infinity

$$\lim_{z\to+\infty} c(z,t) = 0 \tag{49}$$

and that either Dirichlet boundary conditions

$$c(0,t) = c_L \tag{50}$$

or Neumann boundary conditions

$$\frac{\partial c}{\partial z}(0,t) = Dc_L \tag{51}$$

are applied at $z = 0$. We require that $\mu > 0$ (ellipticity condition) and $u > 0$. In this case, the Dirichlet datum at $z = 0$ corresponds to an inflow boundary condition, which guarantees well-posedness for the hyperbolic part. We analyze several possible space discretizations, in order to determine which one shows the best stability properties and can therefore be chosen for the extended DG scheme in conjunction with the Legendre basis in the finite sub-domain. As done in [7] for the pure advection problem, we discretize the PDE system (48) in space, obtaining, after substitution of the discretization of the second equation in (48) into the first, a system of ordinary differential equations of the form

$$\frac{d\mathbf{c}}{dt} = \mathbf{A}\mathbf{c} + \mathbf{g}, \tag{52}$$

where $\mathbf{c}$ is the unknown vector of the expansion of the solution and $\mathbf{g}$ contains the contribution of boundary conditions at $z = 0$, and we study the eigenvalue structure of the matrix $\mathbf{A}$. The corresponding discretization scheme is stable if all the eigenvalues have non-positive real part.
We analyse the following discretizations:

- *Weak form.* We multiply (48) by a test function, integrate by parts and use either Gauss-Laguerre-Radau (GLR) or Gauss-Laguerre (GL) quadrature rules. Two different approaches are possible. In a modal approach, entries of the unknown vector $\mathbf{c}$ are the coefficients of the expansion of the solution in the orthogonal basis of Laguerre functions or Laguerre polynomials. In a nodal approach, the basis functions are the Lagrange basis functions associated with the integration nodes, so that the unknown vector contains the nodal values of the approximate solution.

  Furthermore, the numerical solution can be expanded in a basis of either scaled Laguerre functions or scaled Laguerre polynomials.

- *Strong form.* In this case we directly discretize the strong formulation (48) using a collocation approach and GLR quadrature rules. This is the only practical choice if Dirichlet boundary conditions have to be imposed, because the GLR nodes include the left endpoint of the semi-infinite subdomain, unlike the GL nodes.

We now summarize some definitions we need to introduce the different variants of the matrix $\mathbf{A}$ and vector $\mathbf{g}$.

For discretizations based on Laguerre functions, we define the matrix $\hat{\mathbf{L}} = \{\hat{l}_{ij}\}$ with entries such that

$$\hat{l}_{ij} = \begin{cases} 1/2 & i = j \\ 1 & j < i \\ 0 & j > i. \end{cases} \tag{53}$$

If discretizations based on Laguerre polynomials are considered instead, we use the matrix $\mathbf{L} = \{l_{ij}\}$ defined as

$$l_{ij} = \begin{cases} 0 & i = j \\ 1 & j < i \\ 0 & j > i \end{cases} \tag{54}$$

For nodal discretizations based on the weak form and on scaled Laguerre functions, we then denote by z_j^β the j-th GLR or GL quadrature node, by $h_j^\beta(z)$ the associated Lagrangian polynomial, by ω_i the i-th quadrature weight, and by $\hat{d}_{ij}^\beta$ the entries of the GLR or GL differentiation matrix $\hat{\mathbf{D}}_\beta$ associated with scaled Laguerre functions, defined as follows:

- GL nodes

$$\hat{d}_{ij}^\beta = \begin{cases} \dfrac{\hat{\mathscr{L}}_M^\beta(z_i^\beta)}{(z_i^\beta - z_j^\beta)\hat{\mathscr{L}}_M^\beta(z_j^\beta)} & i \neq j \\ -\dfrac{M+2}{2z_i^\beta} & i = j \end{cases} \tag{55}$$

- GLR nodes

$$\hat{d}_{ij}^\beta = \begin{cases} \dfrac{\hat{\mathscr{L}}_{M+1}^\beta(z_i^\beta)}{(z_i^\beta - z_j^\beta)\hat{\mathscr{L}}_{M+1}^\beta(z_j^\beta)} & i \neq j \\ 0 & i = j \neq 0 \\ -\beta\dfrac{M+1}{2} & i = j = 0. \end{cases} \tag{56}$$

We also define as $\hat{\mathbf{\Omega}}_\beta$ the diagonal matrix with the quadrature weights $\hat{\omega}_i^\beta$ on the diagonal. For a nodal discretization based on Laguerre polynomials, instead, the differentiation matrix $\mathbf{D}_\beta$ has entries d_{ij}^β defined as:

- GL nodes

$$d_{ij}^\beta = \begin{cases} \dfrac{\mathscr{L}_M^\beta(z_i^\beta)}{(z_i^\beta - z_j^\beta)\mathscr{L}_M^\beta(z_j^\beta)} & i \neq j \\ \\ \dfrac{\beta z_i^\beta - M - 2}{2z_i^\beta} & i = j \end{cases} \tag{57}$$

- GLR nodes

$$d_{ij}^\beta = \begin{cases} \dfrac{\mathscr{L}_{M+1}^\beta(z_i^\beta)}{(z_i^\beta - z_j^\beta)\mathscr{L}_{M+1}^\beta(z_j^\beta)} & i \neq j \\ \\ \dfrac{\beta}{2} & i = j \neq 0 \\ \\ -\beta\dfrac{M}{2} & i = j = 0 \end{cases} \tag{58}$$

We also set

$$\hat{\mathbf{g}}_\mathbf{1} = [(\hat{h}_0^\beta)''(z_1), \ldots, (\hat{h}_0^\beta)''(z_M)],\ \hat{\mathbf{g}}_\mathbf{2} = [(\hat{h}_0^\beta)'(z_1), \ldots, (\hat{h}_0^\beta)'(z_M)],$$
$$\mathbf{g}_\mathbf{1} = [(h_0^\beta)''(z_1), \ldots, (h_0^\beta)''(z_M)],\ \mathbf{g}_\mathbf{2} = [(h_0^\beta)'(z_1), \ldots, (h_0^\beta)'(z_M)],$$
$$\hat{\mathbf{h}} = [\hat{h}_0^\beta(0), \ldots, \hat{h}_M^\beta(0)],\ \mathbf{h} = [h_0^\beta(0), \ldots, h_M^\beta(0)],$$
$$\widehat{\mathbf{W}} = \hat{\mathbf{\Omega}}_\beta^{-1}\hat{\mathbf{D}}_\beta^T\hat{\mathbf{\Omega}}_\beta,\ \mathbf{W} = \mathbf{\Omega}_\beta^{-1}\mathbf{D}_\beta^T\mathbf{\Omega}_\beta,$$
$$\hat{\mathbf{r}} = \hat{\mathbf{\Omega}}_\beta^{-1}\hat{\mathbf{h}},\ \mathbf{r} = \mathbf{\Omega}_\beta^{-1}\mathbf{h},$$
$$\mathbf{e} = [1, \ldots, 1]^T \in \mathbf{R}^{M+1}.$$

We also denote by $(\hat{\mathbf{D}}_\beta)_M$ for scaled Laguerre functions, and by $(\mathbf{D}_\beta)_M$ for scaled Laguerre polynomials, the matrices obtained from the differentiation matrices $\hat{\mathbf{D}}_\beta$ and $\mathbf{D}_\beta$ by removing the first row and the first column. Finally we denote by $(\hat{\mathbf{D}}_\beta)_0$ for scaled Laguerre functions, and $(\mathbf{D}_\beta)_0$ for scaled Laguerre polynomials, the matrices obtained from $\hat{\mathbf{D}}_\beta$ and $\mathbf{D}_\beta$ by replacing the first row with zeros.

The expressions of matrix $\mathbf{A}$ and right-hand side $\mathbf{g}$ for the derived discretizations are summarized in Table 10 – note the two use of the matrix $\hat{\mathbf{L}}$ (53) for scaled Laguerre functions and $\mathbf{L}$ (54) for scaled Laguerre polynomials.

Table 10: Definition of matrix $\mathbf{A}$ and vector $\mathbf{g}$ in the Laguerre discretization of (39) or (48) for several formulations 'Form', basis functions 'BF' and boundary conditions 'BC'. 'Coll': collocation, 'Nod': nodal, 'Mod': modal, 'Dir': Dirichlet, 'Neu': Neumann, 'LF': Scaled Laguerre Functions, 'LP': Scaled Laguerre Polynomials. See text for symbol definitions.

Form	BF	BC	$\mathbf{A}$	$\mathbf{g}$
Coll	LF	Dir	$\mu(\hat{\mathbf{D}}_\beta^2)_M - u(\hat{\mathbf{D}}_\beta)_M$	$\mu c_L \hat{\mathbf{g}}_\mathbf{1} - u c_L \hat{\mathbf{g}}_\mathbf{2}$
Coll	LF	Neu	$\mu\hat{\mathbf{D}}_\beta(\hat{\mathbf{D}}_\beta)_0 - u(\hat{\mathbf{D}}_\beta)_0$	$\mu D c_L \hat{\mathbf{g}}_\mathbf{2} - u D c_L \mathbf{e}_\mathbf{1}$
Coll	LP	Dir	$\mu(\mathbf{D}_\beta^2)_M - u(\mathbf{D}_\beta)_M$	$\mu c_L \mathbf{g}_\mathbf{1} - u c_L \mathbf{g}_\mathbf{2}$
Coll	LP	Neu	$\mu\mathbf{D}_\beta(\mathbf{D}_\beta)_0 - u(\mathbf{D}_\beta)_0$	$\mu D c_L \mathbf{g}_\mathbf{2} - u D c_L \mathbf{e}_\mathbf{1}$
Nod	LF	Dir	$-\mu\hat{\mathbf{D}}_\beta\hat{\mathbf{W}} + u\hat{\mathbf{W}}$	$-\mu c_L \hat{\mathbf{D}}_\beta \hat{\mathbf{r}} + u c_L \hat{\mathbf{r}}$
Nod	LF	Neu	$-\mu\hat{\mathbf{\Omega}}_\boldsymbol{\beta}^{-1}\hat{\mathbf{D}}_\beta^T\hat{\mathbf{\Omega}}_\beta\hat{\mathbf{D}}_\beta - u\hat{\mathbf{D}}_\beta$	$-\mu D c_L \hat{\mathbf{r}}$
Nod	LP	Dir	$-\mu\mathbf{D}_\beta\mathbf{W} + \mu\beta\mathbf{D}_\beta + u\mathbf{W} - u\beta\mathbf{I}$	$-\mu c_L \mathbf{D}_\beta \mathbf{r} + u c_L \mathbf{r}$
Nod	LP	Neu	$-\mu\mathbf{W}\mathbf{D}_\beta + \mu\beta\mathbf{D}_\beta - u\mathbf{D}_\beta$	$-\mu D c_L \mathbf{r}$
Mod	LF	Dir	$-\mu\beta^2\hat{\mathbf{L}}^T\hat{\mathbf{L}} - u\beta\hat{\mathbf{L}}$	$\mu\beta^2 c_L \hat{\mathbf{L}}^T\mathbf{e} + u\beta c_L \mathbf{e}$
Mod	LF	Neu	$-\mu\beta^2\hat{\mathbf{L}}\hat{\mathbf{L}}^T + u\beta\hat{\mathbf{L}}^T$	$-\mu\beta D c_L \mathbf{e}$
Mod	LP	Dir	$-\mu\beta^2\mathbf{L}^T(\mathbf{L}+\mathbf{I}) - u\beta(\mathbf{L}+\mathbf{I})$	$u\beta c_L \mathbf{e}$
Mod	LP	Neu	$-\mu\beta^2(\mathbf{L}+\mathbf{I})\mathbf{L}^T + u\beta\mathbf{L}^T$	$-\mu\beta D c_L \mathbf{e}$

As customary for the advection-diffusion problem, the stability property can be a function of the Péclet number, which is usually defined as $Pe = u\mathcal{L}/\mu$, where $\mathcal{L}$ is a reference length scale. For simplicity we choose the length scale $\mathcal{L} = 1$, set $\mu = 1$ and analyze the stability of $\mathbf{A}$ for a fixed value of Pe; the corresponding ranges for β are shown in Table 11 for both scaled Laguerre functions and polynomials.

Table 11: Stability of $\mathbf{A}$ as a function of β: condition under which the largest real part of the eigenvalues is non-positive. $q = 50$, $\mu = 1$. 'Neu': Neumann b.c., 'Dir': Dirichlet b.c., 'LF': Scaled Laguerre Functions, 'LP': Scaled Laguerre Polynomials.

			LF		LP	
			Neu	Dir	Neu	Dir
Strong			$\forall\beta$	$\forall\beta$	$\beta \le 2.6Pe$	$\beta \le 3Pe$
Weak	Nodal	GLR	$\beta \ge 0.58Pe$	$\forall\beta$	$0.017Pe \le \beta \le 2.83Pe$	$\beta \le 3Pe$
		GL	$\beta \ge 2Pe$	$\forall\beta$	$0.25Pe \le \beta \le 2Pe$	$\beta \le 8.5Pe$
	Modal		$\beta \ge 0.58Pe$	$\forall\beta$	$0.017Pe \le \beta \le 2.83Pe$	$\beta \le 3Pe$

It can be observed that only the strong form discretizations based

on Laguerre functions are stable for all boundary conditions and independently of the value of the Péclet number. Other discretizations based on Laguerre functions are instead stable under mild conditions on the value of β as a function of the Péclet number. These conditions become problematic only in the very large Péclet number limit.

In this paper, only the weak form modal discretization based on Laguerre functions was considered for the extended DG scheme, due to its hierarchical nature, that allows in principle for an easy (and if necessary, dynamic) adjustment of the number of basis functions to perform $p-$adaptation. The strong form nodal discretization based on Laguerre functions seems otherwise the most robust option and will be further studied as a basis for extended DG approaches in future work. Discretizations based on Laguerre polynomials are instead only stable under more restrictive conditions, which also affect the choice of β in the small Péclet number case. These conclusions complement the results in [7], where the pure advection problem was discussed. Such an analysis does not seem to have been carried out in the literature, to the best of the authors' knowledge.

References

[1] R.A. Akmaev. Whole atmosphere modeling: Connecting terrestrial and space weather. *Reviews of Geophysics*, 49, 2011.

[2] D. Appelö and T. Colonius. A high-order super-grid-scale absorbing layer and its application to linear hyperbolic systems. *Journal of Computational Physics*, 228(11):4200–4217, 2009.

[3] D.N. Arnold. An interior penalty finite element method with discontinuous elements. *SIAM Journal of Numerical Analysis*, 19:742–760, 1982.

[4] D.N. Arnold, F. Brezzi, B. Cockburn, and L.D. Marini. Unified analysis of discontinuous Galerkin methods for elliptic problems. *SIAM Journal of Numerical Analysis*, 39:1749–1779, 2002.

[5] R.J. Astley. Infinite elements for wave problems: a review of current formulations and an assessment of accuracy. *International Journal of Numerical Methods in Engineering*, 49(7):951–976, 2000.

[6] T. Benacchio and L. Bonaventura. Absorbing boundary conditions: a spectral collocation approach. *International Journal of Numerical Methods in Fluids*, 72(9):913–936, 2013.

[7] T. Benacchio and L. Bonaventura. An extension of DG methods for hyperbolic problems to one-dimensional semi-infinite domains. *Applied Mathematics and Computation*, 350:266–282, 2019.

[8] K. Black. Spectral elements on infinite domains. *SIAM Journal of Scientific Computing*, 19:1667–1681, 1998.

[9] L. Bonaventura. A Semi–implicit Semi–Lagrangian Scheme Using the Height Coordinate for a Nonhydrostatic and Fully Elastic Model of Atmospheric Flows. *Journal of Computational Physics*, 158(2):186–213, 2000.

[10] L. Bonaventura, E.D. Fernández-Nieto, J. Garres-Díaz, and G. Narbona-Reina. Multilayer shallow water models with locally variable number of layers and semi-implicit time discretization. *Journal of Computational Physics*, 364:209–234, 2017.

[11] J.R. Dea. An experimental adaptation of Higdon-type nonreflecting boundary conditions to linear first-order systems. *Journal of Computational and Applied Mathematics*, 235:1354–1366, 2011.

[12] B. Engquist and A. Majda. Absorbing boundary conditions for numerical simulation of waves. *Mathematics of Computation*, 31(139):629–651, 1977.

[13] K. Gerdes. A review of infinite element methods for exterior Helmholtz problems. *Journal of Computational Acoustics*, 8(1):43–62, 2000.

[14] F.X. Giraldo, J.F. Kelly, and E.M. Constantinescu. Implicit-explicit formulations of a three-dimensional nonhydrostatic unified model of the atmosphere (NUMA). *SIAM Journal on Scientific Computing*, 35, 2013.

[15] M. Israeli and S.A. Orszag. Approximation of Radiation Boundary Conditions. *Journal of Computational Physics*, 41:115–135, 1981.

[16] D.R. Jackson, T.J. Fuller-Rowell, D.J. Griffin, M. J. Griffith, C. W. Kelly, D. R. Marsh, and M. T. Walach. Future directions for whole atmosphere modeling: Developments in the context of space weather. *Space Weather*, 17:1342–1350, 2019.

[17] J.B. Klemp and D.R. Durran. An Upper Boundary Condition Permitting Internal Gravity Wave Radiation in Numerical Mesoscale Models. *Journal of Atmospheric Sciences*, 111:430–444, 1983.

[18] J.B. Klemp and D.K. Lilly. Numerical Simulation of Hydrostatic Mountain Waves. *Journal of Atmospheric Sciences*, 35:78–107, 1978.

[19] P.J. Rasch. Toward atmospheres without tops: Absorbing upper boundary conditions for numerical models. *Quarterly Journal of the Royal Meteorological Society*, 112:1195–1218, 1986.

[20] B. Rivière. *Discontinuous Galerkin Methods for Solving Elliptic and Parabolic Equations: Theory and Implementation*. SIAM, 2008.

[21] J. Shen. Stable and efficient spectral methods in unbounded domains using Laguerre functions. *SIAM Journal on Numerical Analysis*, 38:1113–1133, 2001.

[22] J. Shen, T. Tang, and L.-L. Wang. *Spectral Methods: Algorithms, Analysis and Applications*, volume 40 of *Springer Series in Computational Mathematics*. Springer, 2011.

[23] J. Shen and L.-L. Wang. Some recent advances on spectral methods for unbounded domains. *Communications in Computational Physics*, 5:195–241, 2009.

[24] F. Vismara. A coupled scheme for the solution of parabolic problems on unbounded domains. Master's thesis, Politecnico di Milano, 2020. Available at: `https://www.politesi.polimi.it/handle/10589/166694` (last accessed 7 December 2020).

[25] Z.-Q. Wang, B.-Y. Guo, and Y.-N. Wu. Pseudospectral method using generalized Laguerre functions for singular problems on unbounded domains. *Discrete and Continuous Dynamical Systems Series B*, 11(4):1019–1038, 2009.

[26] M.F. Wheeler. An elliptic collocation-finite element method with interior penalties. *SIAM Journal of Numerical Analysis*, 15:152–161, 1978.

[27] Q. Zhuang, J. Shen, and C. Xu. A coupled Legendre–Laguerre spectral–element method for the Navier–Stokes equations in unbounded domains. *Journal of Scientific Computing*, 42(1):1–22, 2010.

MOX Technical Reports, last issues

Dipartimento di Matematica
Politecnico di Milano, Via Bonardi 9 - 20133 Milano (Italy)

81/2020 Antonietti, P. F.; Mascotto, L.; Verani, M.; Zonca, S.
Stability analysis of polytopic Discontinuous Galerkin approximations of the Stokes problem with applications to fluid-structure interaction problems

80/2020 Zingaro, A.; Dede', L.; Menghini, F.; Quarteroni, A.
Hemodynamics of the heart's left atrium based on a Variational Multiscale-LES numerical model

78/2020 Regazzoni, F.; Salvador, M.; Africa, P.c.; Fedele, M.; Dede', L.; Quarteroni, A.
A cardiac electromechanics model coupled with a lumped parameters model for closed-loop blood circulation. Part II: numerical approximation

79/2020 Regazzoni, F.; Salvador, M.; Africa, P.c.; Fedele, M.; Dede', L.; Quarteroni, A.
A cardiac electromechanics model coupled with a lumped parameters model for closed-loop blood circulation. Part I: model derivation

77/2020 Parolini, N.; Ardenghi, G.;Dede’, L.; Quarteroni, A.
A Mathematical Dashboard for the Analysis of Italian COVID-19 Epidemic Data

76/2020 Centofanti, F.; Lepore, A.; Menafoglio, A.; Palumbo, B.; Vantini, S.
Functional Regression Control Chart

75/2020 F. Dassi; A. Fumagalli; D. Losapio; S. Scialò; A. Scotti; G. Vacca
The mixed virtual element method for grids with curved interfaces

74/2020 Formaggia, L; Fumagalli, A.; Scotti, A.
A multi-layer reactive transport model for fractured porous media

73/2020 Bennati, L.; Vergara, C.; Domanin, M.; Trimarchi, S.; Malloggi, C.; Silani, V.; Parati, G.; Casa
A computational fluid structure interaction study for carotids with different atherosclerotic plaques

72/2020 Belli E.; Vantini S.
Measure Inducing Classification and Regression Trees for Functional Data